Rare Met.
DOI 10.1007/s12598-014-0418-9
RARE METALS
www.editorialmanager.com/rmet

# Electrochemical performance of $Al_2O_3$ pre-coated spinel $LiMn_2O_4$

**Hong-Ming Zhou*, Yu-Hua Zhu, Jian Li,**
**Wen-Jiao Sun, Zhong-Zhong Liu**

Received: 28 November 2013 / Revised: 24 December 2013 / Accepted: 26 November 2014

**Abstract** $Al_2O_3$-coated spinel $LiMn_2O_4$ cathode materials, presintered $LiMn_2O_4$ (P-LMO), and calcined $LiMn_2O_4$ (C-LMO) were synthesized by chemical deposition and thermal treating method using presintered and calcined $LiMn_2O_4$ as precursors. The crystal structure, morphology, the thickness of the coating layer, and particle size of prepared samples were investigated by X-ray diffraction (XRD), scanning electron microscopy (SEM), high-resolution transmission electron microscopy (HRTEM), and Malvern instruments. The average particle size of P-LMO with like-spheres (0.3 μm) is much smaller than that of C-LMO (0.5 μm). The $Al_2O_3$ layer of P-LMO can effectively reduce the charge transfer resistance and inhibit the Mn dissolution. The electrochemical performance of P-LMO is better than that of C-LMO. It is found that the $LiMn_2O_4$ cathode materials have excellent electrochemical cyclability by coated 2 mol% $Al_2O_3$ at the surface of presintered material. The initial discharge capacity of the material with 2 mol% $Al_2O_3$-coated is 114.0 $mAh\cdot g^{-1}$ at 0.1C rate and 55 °C, and the capacity retention is 87.3 % at 0.5C rate.

**Keywords** Cathode materials; Lithium manganese oxide; Pre-coated; Aluminum oxide; Cycling stability

## 1 Introduction

Spinel $LiMn_2O_4$, owing to its easy preparation, economic, and environmental advantages, is considered to be a promising material for the positive electrode of secondary lithium batteries [1–3]. The compound has significant advantages in terms of toxicity and cost over $LiCoO_2$. Moreover, the natural abundance of manganese and the familiarity of battery manufacturer with the chemistry of manganese oxides, used in primary alkaline cells [4], made the choice of $LiMn_2O_4$ even more attractive.

The capacity of spinel $LiMn_2O_4$, however, fades rapidly during charge/discharge cycling, which seriously hinders the commercial application of spinel $LiMn_2O_4$ materials. Several possible reasons were proposed to contribute to this fading, such as Jahn–Teller distortion [5], dissolution of spinel into the electrolyte, and decomposition of the electrolyte [6] during cycling and oxygen loss from the spinel lattice of cathode material [7]. Extensive studies were directed toward various strategies to overcome the capacity fading problem of $LiMn_2O_4$. Elemental substitution of Mn with transition metals, such as Zr, Co, Al, Cr, Ni, Mg, etc. [8–12], was proven to be an effective method. However, the improved capacity retention is usually realized at the expense of the decrease of specific capacity.

Morphology, surface chemistry, surface species of the cathodes and the interface between cathodes and electrolyte are of great importance to the electrochemical performance of lithium-ion batteries. Oxides such as MgO, $TiO_2$, $CeO_2$, ZnO, $ZrO_2$, and $Al_2O_3$ [13–17], were studied to suppress capacity fading, indicating that the effectiveness of surface modification on spinel $LiMn_2O_4$. $Al_2O_3$ was improved to be one of the surface coating materials for lithium-ion batteries because of its various advantages such as low cost, excellent chemical stability, and high

---

H.-M. Zhou*, Y.-H. Zhu, J. Li, W.-J. Sun, Z.-Z. Liu
School of Materials Science and Engineering, Central South University, Changsha 410083, China
e-mail: ipezhm@163.com

H.-M. Zhou, J. Li
Hunan Zhengyuan Institute for Energy Storage Materials and Devices, Changsha 410083, China

electronic conductivity possessed by amphoteric oxides [18]. Currently, most of the studies focus on the coating methods of $Al_2O_3$. Tu et al. [19] reported that the $Al_2O_3$ layer was coated through a melting impregnation method, and Kim et al. [20] found $Al_2O_3$ could coat on the spinel $LiMn_2O_4$ by electrostatic attraction forces. On the basis of preliminary studies, $Al(OH)_3$ layer was prepared on the surface of presintered $LiMn_2O_4$ by a chemical deposition method, and then it was thermally treated to form $Al_2O_3$ layer. The $Al_2O_3$ layer can inhibit the growth of $LiMn_2O_4$ during the progress of calcination and reduce the particle size. Moreover, the layer can effectively isolate the $LiMn_2O_4$ and electrolyte, reduce the contact area and diffusion of Mn in the electrolyte, and further improve the electrochemical performance of spinel $LiMn_2O_4$ cathode materials. However, there are few reports on the preparation of $Al_2O_3$-coated $LiMn_2O_4$ using the presintered $LiMn_2O_4$ as precursor. In this work, presintered $LiMn_2O_4$(P-LMO) and calcined $LiMn_2O_4$(C-LMO) coated with different amounts of $Al_2O_3$ were prepared, and the effects of $Al_2O_3$ coating on the electrochemical cycling performances of $LiMn_2O_4$ were systematically studied.

## 2 Experimental

$LiMn_2O_4$ was synthesized by solid-state method. The stoichiometric amounts of $Li_2CO_3$ and electrochemically prepared manganese dioxide (EMD) were firstly mixed in ball grinding mill for 16 h. After the mixture was dried at 80 °C, it was sintered at 500 °C for 6 h to obtain presintered $LiMn_2O_4$, and then calcined at 750 °C for 6 h to gain calcined $LiMn_2O_4$.

The $Al_2O_3$ coating level was controlled at 2 mol% and 5 mol%, and the preparation process of coating solution was conducted as follows. Certain amounts of presintered $LiMn_2O_4$ and calcined $LiMn_2O_4$ were homogeneously dispersed in the absolute ethyl alcohol, respectively. The solutions of aluminum nitrate and aqueous ammonia were slowly added into the dispersion successively drop by drop with electromagnetic stirring in a water bath at 80 °C for several hours, and then $Al(OH)_3$-coated presintered $LiMn_2O_4$ and calcined $LiMn_2O_4$ were obtained, respectively, after the solution was evaporated. Finally, the $Al(OH)_3$-coated presintered $LiMn_2O_4$ and calcined $LiMn_2O_4$ powers were annealed in air at 750 and 350 °C for 10 h, respectively, to obtain $Al_2O_3$-coated $LiMn_2O_4$. According to different $Al_2O_3$ coating amounts, pristine $LiMn_2O_4$, $Al_2O_3$ cal-coated $LiMn_2O_4$, and $Al_2O_3$ pre-coated $LiMn_2O_4$ were labeled as LMO, C-LMO-2, C-LMO-5, P-LMO-2, and P-LMO-5.

The working electrode was prepared by pressing a mixing of the cathode active material, conductive material (acetylene black), and binder (PVDF) in a weight ratio of 80/10/10. The slurry was then pasted on the aluminum foil current collector and dried at 120 °C under vacuum for overnight. The Li metal was used as the counter and reference electrodes. The electrolyte consisted of 1 $mol \cdot L^{-1}$ solution of $LiPF_6$ dissolved in an ethylene/diethyl carbonate (EC/DEC, 1:1 ratio by volume). The cells were assembled in argon-filled dry box in which both the moisture and the oxygen levels were less than $1 \times 10^{-6}$.

Power X-ray diffraction (XRD, SIEMENSD-500) using Cu Kα radiation was used to examine the crystalline phase and the evolution lattice parameters of the prepared material. The surface morphology and microstructure of powers were characterized by scanning electron microscopy (SEM, Sirion 200) and high-resolution transmission electron microscopy (HRTEM, JEM-2100F). The distribution of solid particles was determined using a ZetaSizer 3,000 dynamic light scattering instrument (Malvern Inc.). Before electrochemical tests, the batteries were aged for 24 h to ensure good soakage. The cells fabricated were cycled galvanostatically at 0.1C and 0.5C in the potential range of 3.3–4.5V. Alternating current (AC) impedance was carried out by applying frequency of $1 \times 10^5$–$1 \times 10^{-2}$ Hz with ac-amplitude of 5 mV. Cyclic voltammogram (CV) measurements were performed on electrochemical workstation with three electrode systems (CHI660C, Shanghai), and the CV curves were recorded at scan rate of 0.1 $mV \cdot s^{-1}$ between 3.3 and 4.5 V (vs. $Li/Li^+$).

In order to investigate the effect of $Al_2O_3$ coating layer on decreasing the dissolution of cathode material, the Mn dissolution experiment was also carried out in this study according to the method given in Ref. [21]. About 10 mg of LMO, P-LMO, and C-LMO were, respectively, immersed in 10 ml of $LiPF_6$-EC/DEC (1 $mol \cdot L^{-1}$, 1:1 volume ratio) electrolyte for 3 days. Then, after separating the cathode material power via filtering through filter paper, the dissolved $Mn^{2+}$ in the electrolyte was extracted into water phase using 10 ml HCl (0.1 $mol \cdot L^{-1}$) acid, and the Mn contents were quantitatively determined by atomic absorption spectroscopy (AAS).

## 3 Results and discussion

### 3.1 Physical characterizations

Figure 1 displays the XRD patterns of the LMO, C-LMO, and P-LMO samples with different $Al_2O_3$ coating amounts. Figure 1 indicates that all of the diffraction peaks correspond to a well-defined spinel structure with space group $Fd3m$, being in good agreement with JCPDS card 88-1,749. The absence of any other peaks in the patterns indicates that amorphous $Al_2O_3$ coating on the surface of the base $LiMn_2O_4$ does not penetrate the spinel matrix.

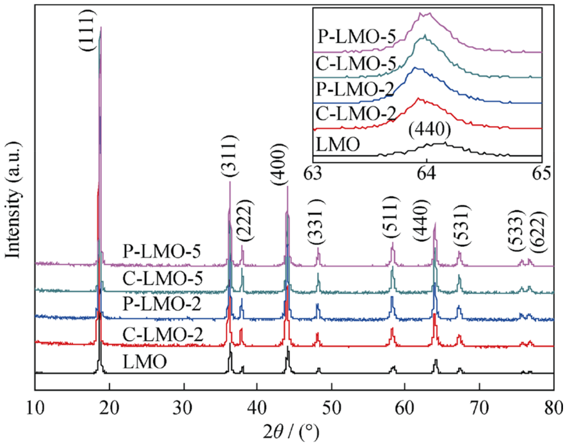

**Fig. 1** XRD patterns of LMO, C-LMO, and P-LMO. Inset showing enlarged diffraction peak of (440)

Compared with the (440) diffraction peak of pristine $LiMn_2O_4$, as shown in the inset of Fig. 1, all the peaks of the $Al_2O_3$-coated $LiMn_2O_4$ exhibit a minute leftward shift, demonstrating that the crystal lattice of $LiMn_2O_4$ is enlarged after coating a layer of $Al_2O_3$. As can be seen from the inset, the lattice constants for both C-LMO and P-LMO increase with the increase of coating amount of $Al_2O_3$. And for the same amount of $Al_2O_3$ surface-modified spinel $LiMn_2O_4$, the (440) diffraction peaks of C-LMO have a further leftward than those of P-LMO, which indicates that P-LMO has smaller lattice parameter. So we suggest that the $Al_2O_3$ layer coated at presintering stage can successfully prohibit grain from growing up. Secondary particles are composed of small grains which further confirm the inhibition of $Al_2O_3$ layer to spinel $LiMn_2O_4$. The particle size measurement of P-LMO-2 and C-LMO-2 was conducted with a laser particle size analyzer.

The particle diameter distributions of P-LMO-2 and C-LMO-2 are presented in Fig. 2. It can be seen from Fig. 2 that the average particle sizes of P-LMO and C-LMO are about 0.30 and 0.50 μm, respectively, and the grain size distribution of P-LMO is more concentrated. It may be attributed to the fact that the grain is growing by intergranular annexed to each other and through the migrating of the grain boundary. Because there is a layer of alumina hydroxide coated at the surface of presintered spinel $LiMn_2O_4$ samples before calcinations, the atoms only can grow up in the cladding layer and not by eating grains outside of the cladding layer during the process of calcinations. This is different from the growing way of $LiMn_2O_4$-coated $Al_2O_3$ after calcinations [22], so the particle diameter of P-LMO is much smaller. This indicates that pre-coated $Al_2O_3$ can reduce the size of particles and also narrow the distribution range of particle size.

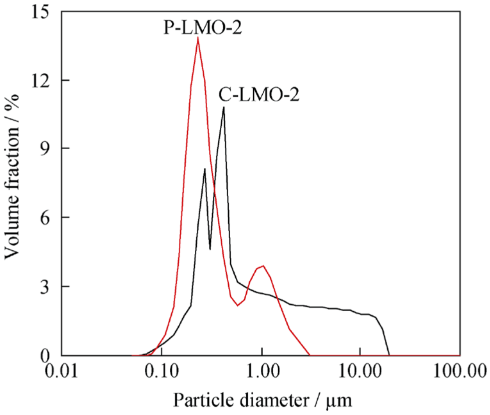

**Fig. 2** Particle diameter distribution of P-LMO-2 and C-LMO-2 powers

The SEM images of the surface morphology of LMO, C-LMO, and P-LMO samples are presented in Fig. 3. The SEM images reveal that the particles of pristine $LiMn_2O_4$ are homogeneously distributed with average particle diameter of 200–300 nm. The border and corner of particles are clearly observed. After surface coating with 2 mol% $Al_2O_3$ (Fig. 3b, c) and 5 mol% $Al_2O_3$ (Fig. 3d, e), the following conclusions can be obtained. Firstly, C-LMO powders exhibit well-developed polyhedral morphology, and the border and corner of the particles are smoother than those of spinel $LiMn_2O_4$. In contrast, the particle morphology of P-LMO shows spherical shape and the clear border and corner of particles disappear. Secondly, the particle size of P-LMO is smaller than that of C-LMO, which is consistent with the results of particle diameter distribution.

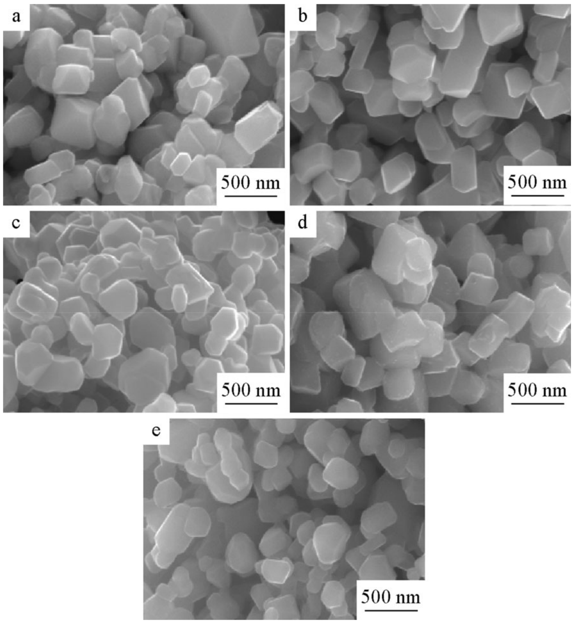

**Fig. 3** SEM images of LMO, C-LMO, and P-LMO powders: **a** LMO, **b** C-LMO-2, **c** P-LMO-2, **d** C-LMO-5, and **e** P-LMO-5

HRTEM was applied to characterize what was changed on the particle surface after surface modification. Figure 4 shows the images of LMO, P-LMO-2, and C-LMO-2 particles. From Fig. 4a, it is evident that $LiMn_2O_4$ grains are submicron particles with good dispersivity. The average size of these particles ranges from 200 to 300 nm. For both coated samples (Fig. 4b–e), core $LiMn_2O_4$ (dark opaque region) can be clearly seen covered by loose thin translucent film. The thickness of the $Al_2O_3$ compact coating layer is around 10 nm. No transition layer can be observed, and the interface between the core and coating layer of C-LMO (Fig. 4d) is obvious. However, the interface between the core and coating layer of P-LMO (Fig. 4e) is unobvious. This may be due to that the $Al(OH)_3$ coating layer of the core presintered $LiMn_2O_4$ gradually diffuses into the $LiMn_2O_4$ crystal and reacts with it, resulting in the formation of solid solution layer during the sintering process. However, the relative intensity of diffraction peaks has no significant change between LMO and P-LMO, indicating that only a small amount $Al^{3+}$ embed into the crystal on the surface of particles, and then the Li–Al–Mn–O solid solution which is similar to a body-doped $LiAl_yMn_{2-y}O_4$ forms on the surface [23].

## 3.2 Electrochemical performance

Figure 5 shows the initial specific discharge capacities of LMO, C-LMO, and P-LMO by applying a current of 0.1C at the potential range of 3.3–4.5 V (vs. $Li/Li^+$) at room temperature.

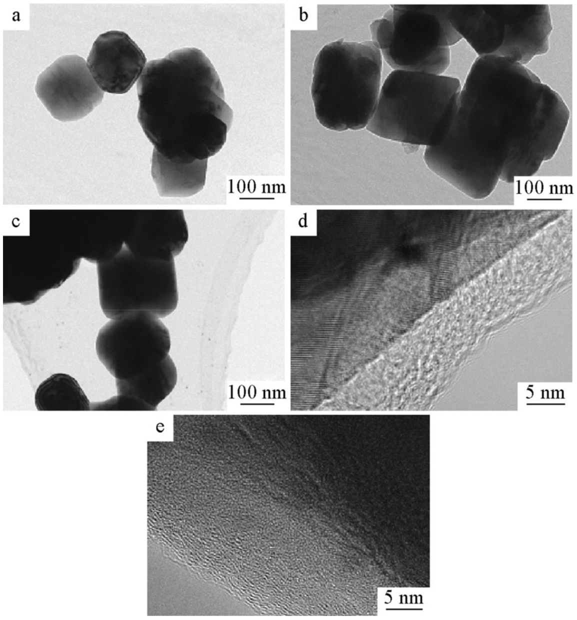

**Fig. 4** TEM images of **a** LMO, **b** and **d** C-LMO-2, **c** and **e** P-LMO-2 powers

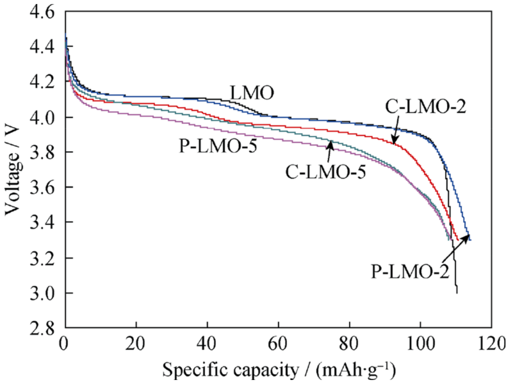

**Fig. 5** Initial specific discharge capacities of LMO, C-LMO, and P-LMO at 0.1C

It can be seen from Fig. 5 that the discharge curves of all samples have two voltage plateaus at approximately 3.9 and 4.1 V. The first plateau at 3.9 V is associated with the single-phase reversible reaction of $LiMn_2O_4 \rightarrow Li_{0.5}Mn_2O_4 + 0.5Li^+$, while the second one at 4.1 V is attributed to the two-phase reaction of $Li_{0.5}Mn_2O_4 \rightarrow Mn_2O_4 + 0.5Li^+$ [21]. The initial discharge capacities of LMO, C-LMO, and P-LMO at room temperature are shown in Table 1. From Table 1, it can be seen that the initial specific discharge capacities of $Al_2O_3$-coated $LiMn_2O_4$ are nearly synonymous with that of LMO. This indicates that the layer of $Al_2O_3$ has no effect on the initial specific discharge capacity of spinel $LiMn_2O_4$, and a small amount of $Al^{3+}$ embedded into the crystal on the surface of P-LMO do not cause the loss of the initial capacity. The two potential plateaus for all P-LMO samples are maintained after 50th cycling, but 5 mol% C-LMO only shows one voltage plateau at the cutoff voltage as shown in Fig. 6. The discharge plateaus of C-LMO descend, and the two platforms integrate gradually during the recycling process. This may be due to that a small amount of $Al^{3+}$ embed into the crystal lattice of $LiMn_2O_4$ and the stronger Al–O bond (bond energy of 512 $kJ \cdot mol^{-1}$) weakens Li–O bond (bond energy of 340.6 $kJ \cdot mol^{-1}$), making the lithium ions more easily spread the 8a-16c-8a channel, so the discharge performance of P-LMO samples is better [24]. However, the layer coated at calcined $LiMn_2O_4$ does not have the above function, and the discharge capacity fades rapidly. This is in part due to the disproportionation reaction of $Mn^{3+}$ in the electrolyte: $Mn^{3+}$ (insoluble) $\rightarrow$ $Mn^{4+}$ (insoluble) + MnO (soluble). The dissolved $Mn^{2+}$ is reduced and deposited on the cathode surface in the form of

**Table 1** Initial specific discharge capacities of LMO, C-LMO, and P-LMO at 0.1C ($mAh \cdot g^{-1}$)

| LMO | C-LMO-2 | P-LMO-2 | C-LMO-5 | P-LMO-5 |
|---|---|---|---|---|
| 110.2 | 110.6 | 114.0 | 107.0 | 109.5 |

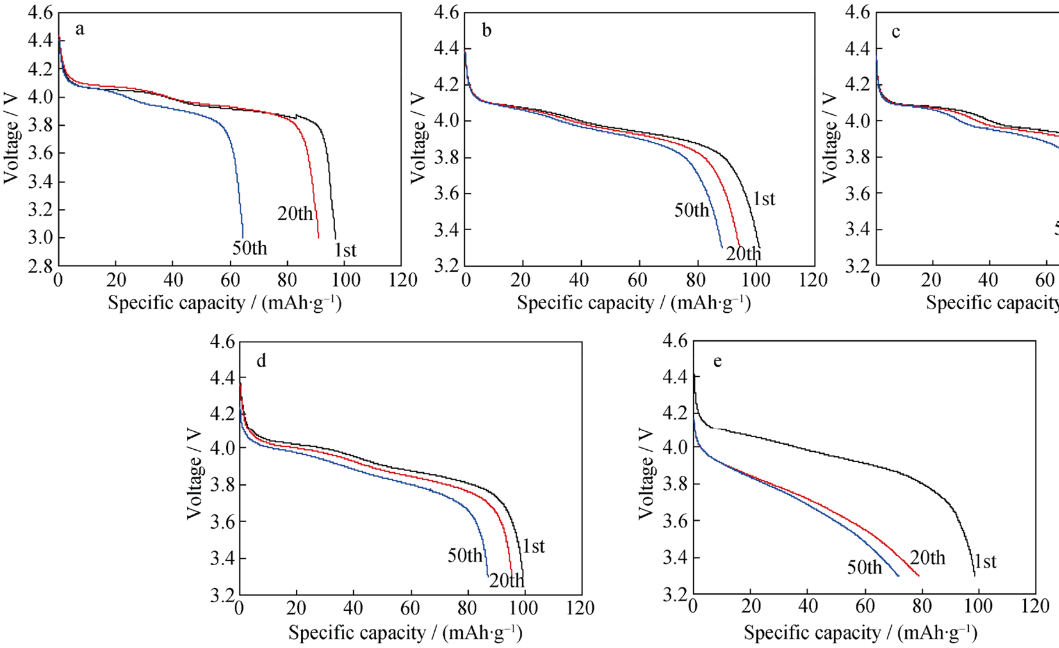

**Fig. 6** Discharge curves of pristine $LiMn_2O_4$- and $Al_2O_3$-coated $LiMn_2O_4$ in voltage of 3.3–4.5 V at 0.5C: **a** LMO, **b** P-LMO-2, **c** C-LMO-2, **d** P-LMO-5, and **e** C-LMO-5

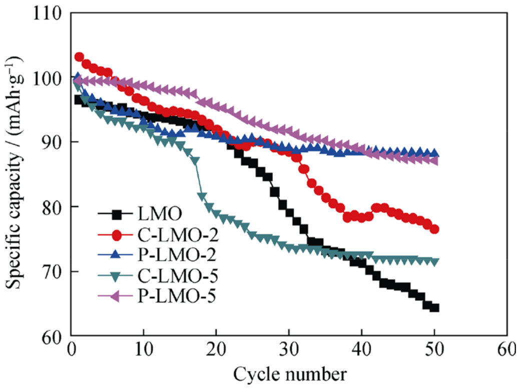

**Fig. 7** Cycling performances of LMO, C-LMO, and P-LMO in voltage of 3.3–4.5 V by applying a current of 0.5C at 55 °C

manganese, which leads to the increase of resistance. And the other part is that the excessive $Al_2O_3$ seriously restraints the insertion and extraction of lithium ions with the increase of $Al_2O_3$ coating amount. Both of them can cause polarization of the charge–discharge curves [25].

Figure 7 shows the cycling performances of LMO, C-LMO, and P-LMO in the voltage range of 3.3–4.5 V by applying a current of 0.5C at 55 °C. As for LMO, the specific discharge capacity fades from 96.7 to 64.4 $mAh{\cdot}g^{-1}$ after 50 cycles, with capacity loss of 33.4 %. In the case of P-LMO, the specific discharge capacities decrease from 100.9 to 88.1 $mAh{\cdot}g^{-1}$ and 99.5 to 86.8 $mAh{\cdot}g^{-1}$ with capacity loss of 12.7 % and 12.8 % for the coating contents of 2 mol% and 5 mol%, respectively. And the capacity loss of corresponding C-LMO is 23.6 % and 27.5 %. Obviously, the cycling performance of P-LMO is superior to those of LMO and C-LMO material. It is attributed to the following reasons: (1) the layer coated at presintering period narrows the particle size range and facilitates the diffusion of lithium ions; 2) the small lattice constants help stabilize the structure of spinel crystal, and thus inhibiting the Jahn–Teller distortion accompanied by the change of electrode material from cubic to tetragonal; 3) the $Al_2O_3$ layer helps improve the valence of Mn ions on the surface of (001) and can effectively reduce the dissolution of $Mn^{3+}$ on the surface of the electrode as well as the chemical reaction between $Mn^{3+}$ and electrolyte [26]. In addition, researches show that P-LMO-2 has a better cycle performance than P-LMO-5, which is due to that the excess $Al_2O_3$ coated at P-LMO-5 will hinder the transportation of lithium ions, leading to the evident decay of the specific capacity.

In order to further understand the difference in their cyclic performance, electrochemical impedance spectroscopy (EIS) of pristine $LiMn_2O_4$- and $Al_2O_3$-coated $LiMn_2O_4$ at the 1st cycle and 50th cycle were measured as shown in Fig. 8. Figure 8a shows the equivalent circuit of the cell to simulate film resistance ($R_f$), charge transfer resistance ($R_{ct}$), Warburg resistance ($Z_w$), and capacitor element (*CPE*). The $R_f$ and $R_{ct}$ data are listed in Table 2. From the results of the 1st cycle, the $R_f$ values of P-LMO and C-LMO are larger than that of LMO due to the combination of the solid electrolyte interface (SEI) and $Al_2O_3$

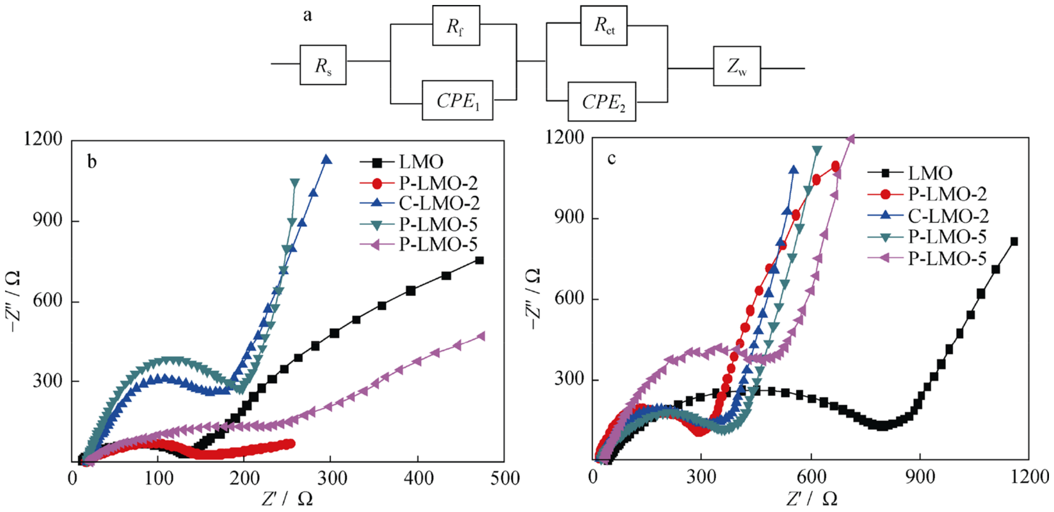

**Fig. 8** Equivalent circuit of cell **a** and EIS results of pristine $LiMn_2O_4$- and $Al_2O_3$-coated $LiMn_2O_4$ at **b** 1st cycle and **c** 50th cycle

**Table 2** $R_f$ and $R_{ct}$ calculation of pristine $LiMn_2O_4$- and $Al_2O_3$-coated $LiMn_2O_4$ at both 1st and 50th cycle based on equivalent circuit of the cell

| Resistance | Cycle | LMO | P-LMO-2 | C-LMO-2 | P-LMO-5 | C-LMO-5 |
|---|---|---|---|---|---|---|
| $R_f$/Ω | 1st cycle | 11.5 | 15.6 | 17.4 | 17.9 | 20.8 |
| | 50th cycle | 42.6 | 19.2 | 22.5 | 24.8 | 32.7 |
| $R_{ct}$/Ω | 1st cycle | 134.5 | 151.1 | 160.3 | 180.1 | 213.7 |
| | 50th cycle | 781.0 | 295.6 | 364.8 | 398.5 | 496.4 |

coating layer on the surface of $LiMn_2O_4$. The charge transfer resistance ($R_{ct}$) of P-LMO has the slowest growth rate; and when the $Al_2O_3$ coating amount is 5 mol%, the $R_{ct}$ grows rapidly for both P-LMO and C-LMO. Similar situations appear in the results of the 50th cycle. This is mainly due to the dissolution of Mn ions, declining the instability of the spinel structure and further resulting in a rapid increase in impedance. However, the $Al_2O_3$ coating layer at the surface of $LiMn_2O_4$ can separate electrolytes and active materials to decrease the decomposition of electrolyte. Particularly, the $LiAl_yMn_{2-y}O_4$ formed on the $LiMn_2O_4$ surface in the P-LMO power strengths the spinel structure and further decreases the growth rate of resistance. In addition, the excess $Al_2O_3$ coated at P-LMO and C-LMO will hinder the transportation of lithium ions, leading to the rise of resistance.

In Fig. 9a and b, the CV profiles of Li/P-LMO-2 were compared with the Li/C-LMO-2 cells in the 1st and 50th cycles at room temperature. Figure 9 indicates that the intervals between the oxidation and the corresponding reduction potential of P-LMO are smaller than those of the C-LMO, indicating that the polarization of the cathode material decreases. CVs for the Li/C-LMO-2 show a distinct shift and broadening of the oxidation and reduction peaks during cycling, indicating a change in the surface structure and composition of the spinel electrode. These changes are likely associated with the rapid capacity losses. By contrast, the CVs of Li/P-LMO-2 show significantly less peak shift and broadening, implying a quick electrode reaction after $Al_2O_3$ pre-coated. The results are consistent with our conclusion that the $Al_2O_3$ pre-coating plays an important role in protecting the electrode surface from chemical attack by acidic electrolyte species, such as HF; thereby, the structural and chemical character of the electrode surface are maintained. In addition, the CVs of C-LMO products appear a redox peak among the voltage of 3.1–3.2 V, while it does not occur in the pre-coated ones. This is mainly attributed to the aluminum hydroxide layer coated at the surface of presintered $LiMn_2O_4$. The layer can effectively avoid the generation of oxygen defects at a high temperature during the calcination process.

AAS results for the Mn dissolution of LMO, C-LMO, and P-LMO cathode materials are given in Fig. 10. The dissolved Mn contents of P-LMO and C-LMO are much lower than that of LMO powers, and that of the P-LMO is the lowest. As a result, it is demonstrated that both cal-coating and pre-coating of $Al_2O_3$ could effectively reduce the dissolution of Mn from the electrode, but the solution-based $Al_2O_3$ pre-coating is more effective in the reduction of the Mn dissolution into the electrolyte.

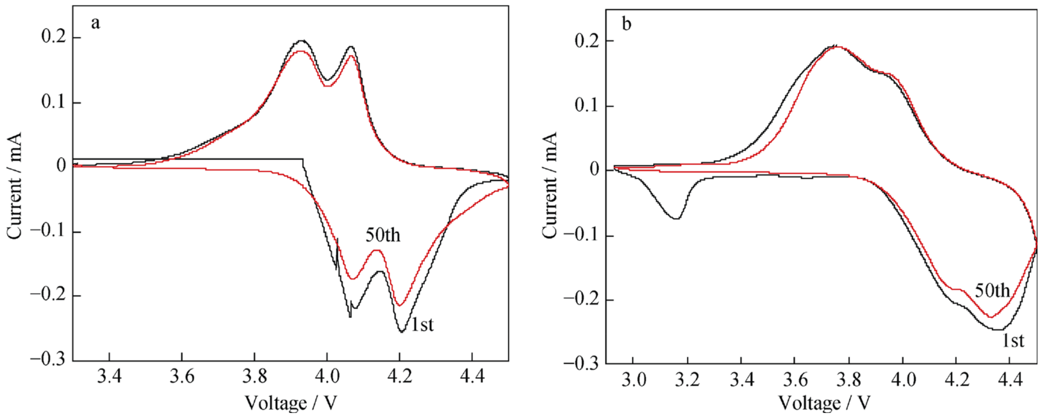

**Fig. 9** CV curves of **a** P-LMO-2 and **b** C-LMO-2 at different cycles measured at room temperature

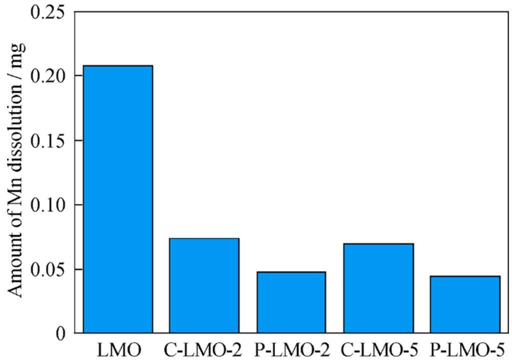

**Fig. 10** AAS results of pristine $LiMn_2O_4$- and $Al_2O_3$-coated $LiMn_2O_4$ spinel cathode materials immersed in $LiPF_6$ with EC/DEC volume ratio of 1:1

### 3.3 Mechanism exploration

Some researchers believed that the fast capacity loss during cycling for spinel $LiMn_2O_4$ was mainly ascribed to the dissolution of manganese from the electrode. HF generated during cycling when using $LiPF_6$-based electrolyte was responsible for the dissolution of the manganese. This chemical reaction was proposed by Myung et al. [27]:

$$LiPF_6 + H_2O \rightarrow LiF + POF_3 + 2HF \qquad (1)$$

HF continuously attacks the active cathode material, and cathode material decomposes as the cycle goes by [28], causing capacity fading

$$2LiMn_2O_4 + 4H^+ \rightarrow 3\lambda\text{-}MnO_2 + 2Li^+ + 2H_2O \qquad (2)$$

Therefore, it is believed that the uniform layer coated at spinel $LiMn_2O_4$ can effectively prevent cathode materials from direct contacting with the electrolyte, reduce the formation of HF, and greatly decrease the capacity loss. The electrochemical data obtained in this study demonstrate that the cycling performance of $LiMn_2O_4$ electrode is significantly improved by pre-coating $Al_2O_3$ layer. The layer coated at the surface of presintered $LiMn_2O_4$ can inhibit the growth of $LiMn_2O_4$ during the further process of calcination and reduce the particle sizes. The small size is contributed to the diffusion of lithium ions. Owing to the decrease of diffusion distance, the utilization of the active material is improved. And P-LMO can also avoid the shortcoming of traditional C-LMO obtained by coating calcined $LiMn_2O_4$, in which the particles near the center of active materials are difficult to use. Moreover, the $Al_2O_3$ layer can effectively decrease the interface area between the cathode and the electrolyte as well as the HF content at the cathode surface.

Pre-coating the spinel $LiMn_2O_4$ with $Al_2O_3$ layer via chemical deposition method results in the improvement of the electrochemical properties.

## 4 Conclusion

Spinel $LiMn_2O_4$ was synthesized by the two-process solid-state method, and the $Al_2O_3$ coating layer was coated on the surface of presintering $LiMn_2O_4$ and calcined $LiMn_2O_4$ by chemical deposition method. $Al_2O_3$ layer forms uniformly on the surface of spinel $LiMn_2O_4$. Compared with C-LMO, P-LMO materials have smaller particle size and show much batter capacity retention at 55 °C, especially the 2 mol% $Al_2O_3$ pre-coated $LiMn_2O_4$. The capacity retention of this material is 87.3 % after 50 cycles. The surface modification with $Al_2O_3$ coated at presintering period in this work acts at least two roles: (1) preventing the particles further excessively growing and facilitating the diffusion of lithium ions through it, and (2) separating electrolytes and active materials and thus preventing the dissolution of the Mn ions to ensure the structure stability. Furthermore, this pre-coated way combined with traditional solid-state method makes the industrialization of cathode material $LiMn_2O_4$ for lithium-ion batteries more prosperous.

**Acknowledgments** This study was financially supported by the Science and Technology Project of Hunan Province (No. 2010FJ4061) and the Technology Project of Changsha (No. K1201039-11).

## References

[1] Xu B, Qian DN, Wang ZY, Meng YS. Recent progress in cathode materials research for advanced lithium ion batteries. Mater Sci Eng. 2012;73(5–6):51.

[2] Wu HM, Tu JP, Chen XT, Li Y, Zhao XB, Cao GS. Electrochemical study on $LiMn_2O_4$ as cathode material for lithium ion batteries. J Electroanal Chem. 2006;586(2):180.

[3] He XM, Li JJ, Cai Y, Jiang CY, Wan CR. Preparation of spherical spinel $LiMn_2O_4$ cathode material for Li-ion batteries. Mater Chem Phys. 2006;95(1):105.

[4] Cabana J, Valdes-Solis T, Palacin MR, Oro-Sole J, Fuertes A, Marban G, Fuertes AB. Enhanced high rate performance of $LiMn_2O_4$ spinel nanoparticles synthesized by a hard-template route. J Power Sources. 2007;166(2):492.

[5] Li XF, Xu YL, Wang CL. Suppression of Jahn-Teller distortion of spinel $LiMn_2O_4$ cathode. J Alloy Compd. 2009;479(1–2):310.

[6] Xiao LF, Zhao YQ, Yang YY, Cao YL, Ai XP, Yang HX. Enhanced electrochemical stability of Al-doped $LiMn_2O_4$ synthesized by a polymer-pyrolysis method. Electrochim Acta. 2008;54(2):545.

[7] Xia YG, Wang HY, Zhang Q, Nakamura H, Noguchi H, Yoshio M. Oxygen deficiency, a key factor in controlling the cycle performance of Mn-spinel cathode for lithium-ion batteries. J Power Sources. 2007;166(2):485.

[8] Oh SH, Chung KY, Jeon SH, Kim CS, Cho WB. Structural and electrochemical investigations on the $LiNi_{0.5\text{-}x}Mn_{1.5\text{-}y}M_{x+y}O_4$ (M = Cr, Al, Zr) compound for 5 V cathode material. J Alloy Compd. 2009;469(1–2):244.

[9] Hwang BJ, Tsai YW, Santhanam R, Wu YW, Hu SG, Lee JF, Liu DG. Evolution of local electronic and atomic structure of Co-doped $LiMn_2O_4$ cathode material for lithium rechargeable batteries. J Power Sources. 2006;123(2):206.

[10] Hwang BJ, Santhanam R, Liu DG, Tsai YW. Effect of Al-substitution on the stability of spinel $LiMn_2O_4$ synthesized by citric acid sol-gel method. J Power Sources. 2001;102(1–2):326.

[11] Wei YJ, Nam KW, Kim KB, Chen G. Spectroscopic studies of the structural properties of Ni substituted spinel $LiMn_2O_4$. Solid State Ion. 2006;177(1–2):29.

[12] Lee KS, Bang HJ, Myung ST, Prakash J, Amine K, Sun YK. Synthesis and electrochemical properties of spherical spinel $Li_{1.05}M_{0.05}Mn_{1.9}O_4$ (M = Mg and Al) as a cathode material for lithium-ion batteries by co-precipitation method. J Power Sources. 2007;174(2):726.

[13] Walz KA, Johnson CS, Genthe J, Stoiber LC, Zeltner WA, Anderson MA, Thackeray MM. Elevated temperature cycling stability and electrochemical impendence of $LiMn_2O_4$ cathodes with nanoporous $ZrO_2$ and $TiO_2$ coating. J Power Sources. 2010;195(15):4943.

[14] Gnanaraj JS, Pol VG, Gedanken A, Aurbach D. Improving the high-temperature performance of $LiMn_2O_4$ spinel electrodes by coating the active mass with MgO via a sonochemical method. Electrochem Commun. 2003;5(11):940.

[15] Eftekhari A. Aluminum oxide as a multi-function agent for improving battery performance of $LiMn_2O_4$ cathode. Solid State Ion. 2004;167(3–4):237.

[16] Tu J, Zhao XB, Xie J, Cao GS, Zhuang DG, Zhu TJ, Tu JP. Enhanced low voltage cycling stability of $LiMn_2O_4$ cathode by ZnO coating for lithium ion batteries. J Alloy Compd. 2007;432(1–2):313.

[17] Ha HW, Yun NJ, Kim K. Improvement of electrochemical stability of $LiMn_2O_4$ by $CeO_2$ coating for lithium-ion batteries. Electrochim Acta. 2007;52(9):3236.

[18] Cui YL, Wu C, Wei T, Shi YL, Zhuang QC, Sun Z. Electrochemical performance of spinel $LiMn_2O_4$ modified. Hemistry. 2011;74(8):742.

[19] Tu J, Zhao XB, Cao GS, Zhuang DG, Zhu TJ, Tu JP. Enhanced cycling stability of $LiMn_2O_4$ by surface modification with melting impregnation method. Electrochim Acta. 2006;51(28):6456.

[20] Kim WK, Han DW, Ryu WH, Lim SJ, Kwon HS. $Al_2O_3$ coating on $LiMn_2O_4$ by electrostatic attraction forces and its effects on the high temperature cyclic performance. Electrochim Acta. 2012;71(5):17.

[21] Halil S, Huseyin G, Saban P, Ahmet U. The effect of LBO coating method on electrochemical performance of $LiMn_2O_4$ cathode material. Solid State Ion. 2008;178(35–36):1837.

[22] Zheng ZQ. Fundamentals of Materials Science. Changsha: Central South University; 2005. 365.

[23] Wang ZX, Xing ZJ, Li XH, Guo HJ, Peng WJ. Study on $Al_2O_3$-modified $LiMn_2O_4$ prepared by heterogeneous nucleation. Acta Phys Chim Sin. 2004;20(8):790.

[24] Xiong LL, Xu YL, Zhang C, Tao T. Doping-coating surface modification of spinel $LiMn_2O_4$ cathode material with $Al^{3+}$ for lithium-ion batteries. Acta Phys Chim Sin. 2012;28(5):1177.

[25] Duan F, Du ZZ, Yang P, Chen P, Zhong SS, Zhang DW. Study of coated as a cathode material for lithium ion batteries. J Hefei Univ Technol (Nat Sci). 2013;36(3):346.

[26] Li XC, Zhang XY, Lu YJ, Li K. Interface reaction mechanism of welding $Al_2O_3$ ceramic with AgCuInTi brazing filler. Chin J Rare Met. 2013;37(1):71.

[27] Myung ST, Izumi K, Komaba S, Sun YK, Yashiro H, Kumagai N. Role of alumina coating on Li-Ni-Co-Mn-O particles as positive electrode material for lithium-ion batteries. Chem Mater. 2005;17(14):3695.

[28] Qing CB, Bai Y, Yang JM, Zhang WF. Enhanced cycling stability of $LiMn_2O_4$ cathode by amorphous $FePO_4$ coating. Electrochim Acta. 2011;56(19):6612.